https://doi.org/10.5194/essd-2026-296
Preprint. Discussion started: 7 July 2026

Open Access Earth System Science Data Discussions

The Cooling Efficiency Factor Index (CEFI): A New Satellite-Based Dataset for Research and Operational Monitoring of Land Surface Processes

Matteo Zampieri[1,2], Marco Girardello[3], Saquib Md Saharwardi[1], Guido Ceccherini[2], Emanuele Massaro[4], Mirco Migliavacca[5], Ibrahim Hoteit[1], Alessandro Cescatti[5]

[1]Department of Physical Science and Engineering, King Abdullah University of Science and Technology, Thuwal 23955, Saudi Arabia
[2]Engineering Ingegneria Informatica S.p.A., Roma 00144, Italy
[3]Department of Geography, Trinity College Dublin, The University of Dublin, Dublin 2, Ireland
[4]European Environment Agency, Copenhagen 1050, Denmark
[5]European Commission, Joint Research Centre (JRC), Ispra, Italy

Correspondence to: Matteo Zampieri (matteo.zampieri@ext.ec.europa.eu) and Alessandro Cescatti (alessandro.cescatti@europa.eu)

Abstract. The cooling efficiency of the land surface, i.e., its ability to dissipate absorbed radiation and moderate temperature rise, is reflected in its apparent heat capacity, a property that varies throughout the day in response to the relative intensities of sensible and latent heat fluxes. Under clear-sky conditions, the daytime increase in apparent heat capacity can be reliably estimated using geostationary satellite data and used to derive a new dataset called Cooling Efficiency Factor Index (CEFI). This index quantifies land surface energy dissipation through turbulent and ecohydrological processes from 2005 to near real time at a spatial resolution of 5 km. The spatial distribution of the CEFI dataset is primarily determined by land cover, water availability, surface roughness, and wind speed. Its temporal variability can be exploited to derive proxies for variables and processes that are otherwise difficult to observe, especially in real time, such as evapotranspiration and wind speed anomalies. Accordingly, the CEFI dataset can serve as an indicator of vegetation drought stress, the condition in which plants close their stomata due to soil water limitation and high atmospheric water demand, as well as vegetation productivity. It can also detect flash droughts and support improved estimation of fire risk in natural ecosystems, crop production losses in agricultural areas, and dust formation in desert regions. In addition, the dataset can be used to quantify the cooling efficiency of urban areas. This paper provides access to a publicly available CEFI dataset updated in near real time. Given its broad range of applications, the dataset can be used for both research and operational monitoring, to constrain poorly observed processes in dynamical models, and as an additional predictor or predictand in machine learning applications.

https://doi.org/10.5194/essd-2026-296
Preprint. Discussion started: 7 July 2026

Open Access Earth System Science Data Discussions

1 Introduction

The land surface is a fundamental component of the Earth system, forming the dynamic interface where exchanges of energy, water, and carbon connect the atmosphere, biosphere, and hydrosphere. It sustains natural ecosystems and provides the physical and ecological basis for agriculture (Mehrabi et al. 2025), forestry (Hansen et al. 2013), and human settlements (Pesaresi et al. 2016). The state of the land surface controls key processes such as evapotranspiration and heat flux partitioning (Jung et al, 2019), thereby regulating local climate anomalies and extremes (Zampieri et al. 2009, Grossiord et al. 2020) as well as global climate change (Novick et al. 2016, Friedlingstein et 2022). Its condition directly influences ecosystem productivity (Ciais et al. 2005, Novick et al. 2024), agricultural production (Brás et al. 2021), and human well-being (Massaro et al. 2023).

The land surface is now experiencing profound and accelerating changes driven by global warming, land-use conversion, intensified climate variability and proximity to tipping points (Jung et al. 2010, Hansen et al. 2013, McKay et al. 2022, Friedlingstein et al. 2022, Mehrabi et al. 2025). Rising temperatures, shifts in precipitation regimes, and increasing frequency of extreme events have altered vegetation dynamics, soil moisture availability and carbon cycle (Reichstein et al. 2013), and surface energy balance (Alkama and Cescatti, 2016; Duveiller et al. 2018). These transformations not only modify regional hydrological cycles and surface temperatures but also generate feedbacks that can amplify or dampen climate anomalies at the local and global scales (Zampieri et al. 2009, Miralles et al. 2014, Naumann et al. 2018, Alkama and Cescatti 2022, Friedlingstein et al. 2022). Understanding how land surface processes respond to these disturbances is essential for predicting ecosystem resilience and ensuring sustainable land and water management (Hartmann et al. 2022).

Given the complexity and scale of these interactions, a robust and continuous monitoring system is required to capture the spatiotemporal variability of land surface behavior. Satellite observations provide an unparalleled means to assess these dynamics at regional to global scales (Li et al. 2023, Pickens et al. 2025). In this context, the Cooling Efficiency Factor Index (CEFI, /ˈsɪfaɪ/ Zampieri et al. 2025) offers a novel approach to quantify the land surface's capacity to dissipate heat through evaporation and other processes. Derived from geostationary satellite data, CEFI enables real time monitoring of surface thermal responses to environmental and climatic drivers.

Here, we show that the CEFI index proposed provides valuable insights into drought stress, vegetation health, wind stress over arid areas, and the thermal regulation of urban environments. The present study describes the conceptual basis and the implementation details of the CEFI as a reference for a publicly available dataset extending from 2005 and updated in near real time. We also illustrate several potential applications of CEFI, showcasing its potential for monitoring vegetation drought stress, assessing surface wind stress in arid environments, estimating fire and dust risk, and evaluating the cooling performance of urban areas. Through these analyses, we highlight the value of CEFI as a versatile indicator for studying land–atmosphere interactions, improving dynamical and machine learning based models and supporting climate adaptation and environmental management strategies.

https://doi.org/10.5194/essd-2026-296
Preprint. Discussion started: 7 July 2026

Open Access Earth System Science Data Discussions

2 Theory

The CEFI definition is extensively discussed and contextualized by Zampieri et al. (2025). A practical example of CEFI computation is provided in Figure 1. In essence, the CEFI formulation is based on the surface energy balance equation (Arya 2001):

$$c_s \, dT_s/dt = R_n - SH - LH - G, \quad (1)$$

where T_s is the land surface temperature (LST, Fig. 1a), expressed in K, c_s is the surface heat capacity ($[c_s]$=W m^{-2} K^{-1}), R_n is the net radiation (Fig. 1b), SH is the sensible heat flux, LH is the latent heat flux and G is the ground heat flux (all expressed in W m^{-2}). Here, T_s and c_s are associated with an infinitesimally thin layer of the surface (either canopy or bare soil), which is emitting the thermal radiation measured by the satellite that is used to define the LST product.

Following Zampieri et al. (2025), Equation 1 can be integrated to give the temperature response between two different times of the day, after the sunrise and before the sunset.

$$\Delta T_s = \int (R_n - SH - LH - G) \, dt / c_s. \quad (2)$$

This equation can be conveniently rearranged to express the heat capacity, disentangling the terms that can be measured from satellite from the unknown terms.

$$c_s = c_a - e_c, \quad (3)$$

where

$$c_a = \int R_n \, dt / \Delta T_s, \quad (4)$$

is the *apparent heat capacity* (Fig. 1d), which can be measured from satellite, and

$$e_c = \int (SH + LH + G) \, dt / \Delta T_s \quad (5)$$

is the *cooling efficiency*, which is considered as an unknown in this framework.

The c_s is found to be very small, especially during the day, when the apparent heat capacity and the cooling efficiency almost balance each other and they increase approximately linearly as a function of ΔT_s (Zampieri et al 2025). This allows to define the *cooling efficiency factor* (CEF ≡ e_{c1}, Eq. 6) as the linear regression of the c_a versus ΔT_s curves displayed in Fig. 1d, as expressed by the following linear approximation:

$$c_a \approx c_s + e_{c0} + e_{c1} \cdot \Delta T_s, \quad (6)$$

where the c_s can be either neglected or incorporated in the e_{c0} term as intercept of the regression lines, which allows to classify the diurnal temperature variability of the land surface with a single number. This is a main advantage of the CEF formulation. Moreover, differently than other satellite products, the CEF error can be precisely quantified through the standard error of the estimated regression slope parameter. Finally, to ensure temporal continuity in the dataset despite days when daily estimation is not possible, the *cooling efficiency factor index* (CEFI) is defined as the monthly median of the available daily CEF estimations.

https://doi.org/10.5194/essd-2026-296
Preprint. Discussion started: 7 July 2026

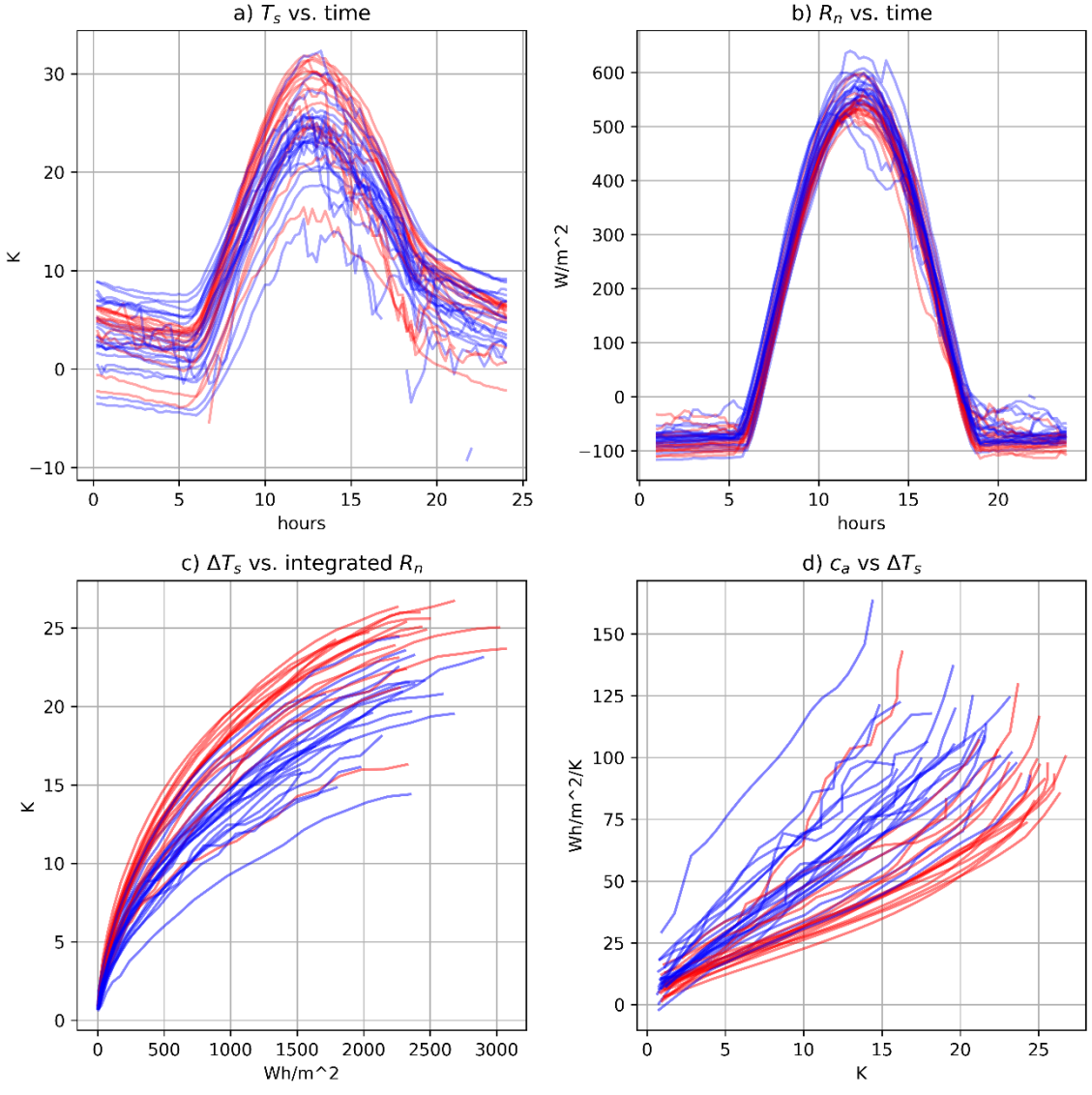

Figure 1: a) LST vs. time, b) net radiation vs. time, c) daytime ΔT_s vs. integrated net radiation; d) apparent heat capacity vs. ΔT_s computed over a forested region in April in Spain (adapted from Zampieri et al. 2025). Red/blue lines correspond to days characterized by dry/normal conditions. Only days with sufficient continuous cloudless conditions are shown.

3 Methods

The apparent heat capacity can be estimated at sub-daily resolution using Eq. (4) using geostationary satellite data from EUMETSAT Land Surface Analysis Satellite Application Facility (LSASAF, https://lsa-saf.eumetsat.int/), which provides

https://doi.org/10.5194/essd-2026-296
Preprint. Discussion started: 7 July 2026

high-frequency land surface temperature (LST) and radiation measurements (downward shortwave radiation every 15 min, downward longwave every 30 min) with constant viewing geometry and pixel size (Trigo et al. 2011). Surface thermal radiation is computed from LST using the Stefan-Boltzmann law. Emissivity and albedo are provided by LSASAF at daily time scale (Trigo et al. 2008). Data cover Africa, Southern Europe, the Arabian Peninsula, and parts of South America from 2005 to near-real time at 0.05°×0.05° resolution. More specifically, the analysis presented in this paper covers a 21 years period from 2005 to 2025.

In Zampieri et al. (2025) gaps in LST up to 45 min are linearly interpolated; larger gaps lead to rejection of that day. For shortwave radiation no gap filling was applied. Only periods with sufficiently long clear-sky conditions (4 hours of continuous data) and monotonically increasing LST are used for linear regression of apparent heat capacity versus ΔLST (Eq. 6) to estimate daily CEF, rejecting regressions with $r^2 < 0.7$. Finally, CEFI was defined at the monthly level as the median of valid daily CEF estimates.

Differently from Zampieri et al. (2025), here we allow small deviations from monotonicity, accepting temperature changes between subsequent acquisitions of at least –0.1 K. We also gap-fill short missing periods in radiation data affecting a single time step, typically due to missing files in the repository. Finally, we permit the estimation of CEF over shorter time windows of 2 hours. These modifications increase the number of valid cases for process studies and monitoring applications, while having a negligible impact on the accuracy of the CEFI estimation.

As in Zampieri et al. (2025), we compare the CEFI with the stress factor estimated by the Global Land Evaporation Amsterdam Model (GLEAM) and with NDVI (Normalized Difference Vegetation Index) from the Moderate Resolution Imaging Spectroradiometer (MODIS, Justice et al. 2002). However, in this study we use a newer and improved version of GLEAM (version 4.2b, Miralles et al. 2025) available at 0.1° spatial resolution, making the analysis more sensitive to fine-scale features than the work that was previously conducted at 0.25°. Similarly, the analysis of NDVI and the other variables is also performed here at higher spatial resolution compared to Zampieri et al. (2025).

Here, we also compare the CEFI to precipitation and Standardized Precipitation Index from Rainfall Estimates from Rain Gauge and Satellite Observations (CHIRPS, https://www.chc.ucsb.edu/data/chirps), to the soil moisture from the European Space Agency (ESA) Climate Change Initiative (https://climate.esa.int/en/projects/soil-moisture/), to the Global Surface Waters datasets of the Joint Research Centre (https://global-surface-water.appspot.com/), to the burned area statistics from MODIS (MCD64A1, https://ladsweb.modaps.eosdis.nasa.gov/missions-and-measurements/products/MCD64A1), to the 10 meter wind taken from the ERA5-Land reanalysis retrieved from the Copernicus Climate Data Store (CDS, https://cds.climate.copernicus.eu/), to crop production records by FAOSTAT (https://www.fao.org/faostat/), to Dust Aerosol Optical Depth (DAOD) from the CAMS global reanalysis (EAC4, ECMWF Atmospheric Composition Reanalysis 4), retrieved from Copernicus Atmosphere Data Store (ADS, https://ads.atmosphere.copernicus.eu/datasets).

Statistical analyses involve mainly standard Pearson correlation coefficient estimation between the CEFI and the other involved dataset. Occasionally we use machine learning approach to reconstruct the CEFI spatial distribution (globally and for cities) and quantify the different features importance. In these cases, the datasets were randomly split into training (80%)

https://doi.org/10.5194/essd-2026-296
Preprint. Discussion started: 7 July 2026

and testing (20%) subsets. A Random Forest (RF) regressor was trained on the training data. Predictions were then generated for the independent test set to evaluate out-of-sample performance. Model performance was assessed using standard regression metrics, including the coefficient of determination (R^2), root mean square error (RMSE), and mean absolute error (MAE). These metrics provide complementary information on the model's ability to explain variance and the magnitude of prediction errors. To further assess the robustness and physical consistency of the model results, partial dependence analysis was conducted, albeit not shown in the main paper. Partial dependence plots (PDPs) were used to quantify the marginal effect of individual predictor variables on the predicted outcome, while averaging out the influence of all other variables. This analysis enabled verification that the modeled relationships were consistent with the expected physical behavior of the system and helped identify potential nonlinearities and interaction effects captured by the model.

4 Results

4.1 Spatial and temporal patterns of the CEFI

4.1.1 CEFI accuracy and spatial variability

The long term mean CEFI spatial distribution (Fig.2a) displays a well-defined spatial variability with high/low values representing high/low cooling efficiency of the land surface. That information is associated to different levels of accuracy that is higher in dry regions and lower in humid regions. In general, a minimum level of accuracy is ensured by the data processing that excludes any acquisition that departs from the linear assumption of the diurnal variations of apparent heat capacity (see Methods). Because of this reason the maximum error of the daily estimations is contained to roughly the 25% on average (Fig. 2b). However, the same procedure reduces the number of valid estimations especially at higher latitudes and the tropics (Fig. 2c). Therefore, we expect a reduced applicability of the CEFI in these regions.

https://doi.org/10.5194/essd-2026-296
Preprint. Discussion started: 7 July 2026

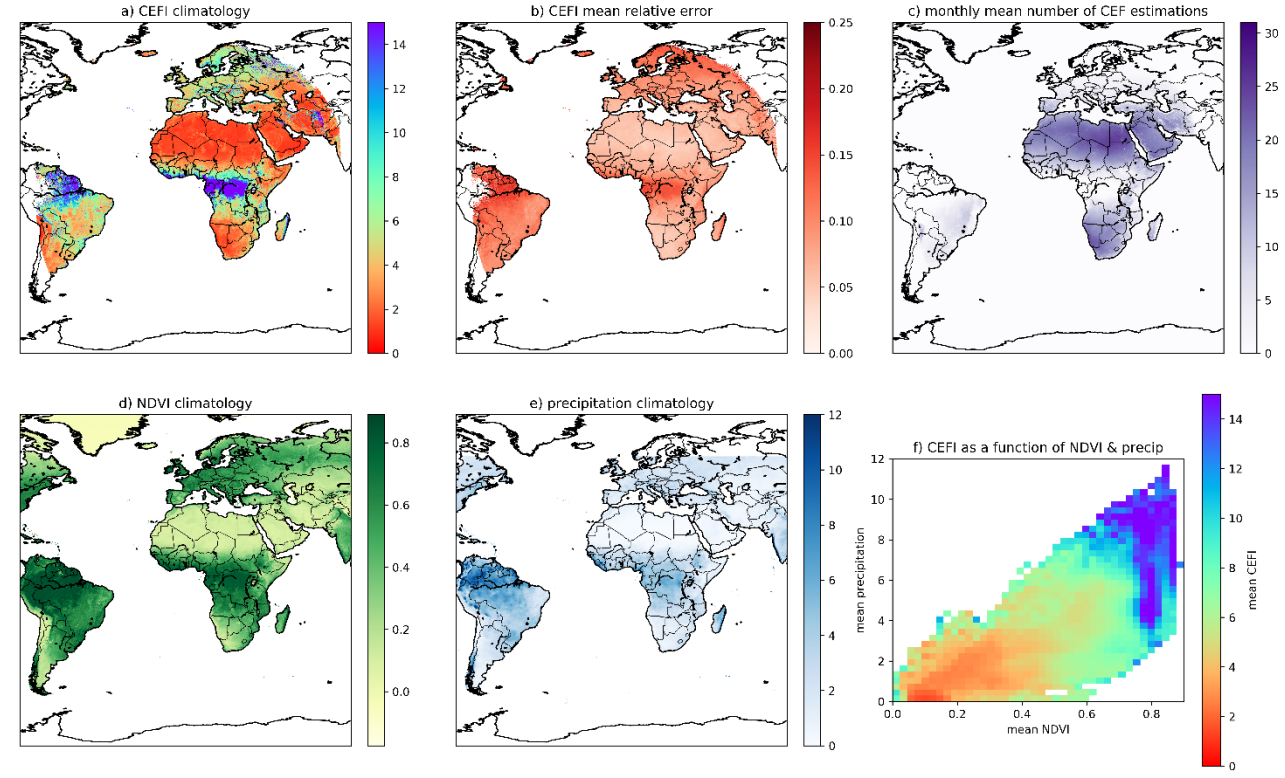

Figure 2: a) CEFI climatology 2005-2025 (Wh m^{-2} K^{-2}), b) mean CEFI relative error, c) monthly mean number of CEF estimation used to define the CEFI, d) NDVI climatology, e) precipitation climatology (mm/day) and f) mean CEFI as a function of mean precipitation and NDVI.

The minimum CEFI of about 1 Wh m^{-2} K^{-2} is found in several regions of the Sahara desert, over the so-called Empty Quarter in the southeast of the Arabian Peninsula (Rub' al Khali), and in the Kalahari desert southwest of Africa. In these regions, because of low cloudiness the accuracy of the estimation is the highest as the error of the CEFI estimation is about the 5% and the monthly mean number of valid CEF estimation is larger than 15. The CEFI values increase to about 3 Wh m^{-2} K^{-2} in transitional regions such as the Mediterranean, the Sahel, East Africa and South Africa still with relatively low error (5 to10%) and 10 to 15 estimations per month. The CEFI reaches about 5 Wh m^{-2} K^{-2} over flat areas of continental Europe and the Subtropical regions of Africa and South America, with associate error of about the 10% and around 5 estimations per month. The CEFI increases to 8-10 Wh m^{-2} K^{-2} over mountainous regions in Central Europe and the Baltic regions (10-15% error, less than 5 estimations per month) and reaches values of about 20 Wh m^{-2} K^{-2} over tropical forests in central Africa and America (15% error, less than 1 estimation per month). The error of the estimation also tend to grow along the margin of the region covered by the geostationary satellite.

https://doi.org/10.5194/essd-2026-296
Preprint. Discussion started: 7 July 2026

The CEFI spatial distribution qualitatively resembles that of vegetation cover (Fig. 2d) and precipitation amount (Fig 2f). However, high CEFI levels are found also in areas with less precipitation, if the local hydrological conditions can support vegetation (Fig 2e). In fact, the average CEFI spatial distribution is mostly related to the distribution of vegetation than that of precipitation or other variables. A simple machine learning regression model (random forest) can explain the 87% of the average CEFI spatial variability (RMSE = 1.16) using as predictors the distribution of NDVI (53.8% explained variance), mean surface wind during the time of the CEFI estimation (11.5%), mean precipitation (11.2%), canopy height standard deviation (7.5%), orography (7.5%), orography standard deviation (4.6%) and surface water fraction (4.0%). The given percentages associated with the individual variables represent their relative contributions to the fraction of total variance explained by the random forest model (i.e. variable importance summing to 100%). The dominance of the vegetation distribution as explaining variable compared to precipitation demonstrate the sensitivity to the CEFI to the evapotranspiration also in regions were vegetation is not only supported by rainfall but also by other components of surface hydrology such as irrigation and groundwater fluxes. Vegetation also acts as an important mediator of evapotranspiration, which directly depends on the leaf area index. Other explaining variables highlight the role of wind and surface roughness in determining the turbulent fluxes defining the cooling efficiency. Surface water fraction here plays a minor role, as the CEFI is not computed over lakes and large water bodies over the land surface.

4.1.2 CEFI temporal variability

The CEFI variability range is quantified by the coefficient of variation (CV ≡ standard deviation divided by the mean). When the coefficient of variation exceeds the relative error, the magnitude of variability is larger than the associated uncertainty, indicating that the signal is likely to be informative rather than noise-dominated. The CV tends to be lower in desert regions (10-20%, Fig. 3a), where the modulation effects related to vegetation are absent, but still higher than the mean estimation error (Fig. 2b). Over such regions, the CEFI CV display limited seasonal variations (Fig 3b). Over vegetated regions, the CEFI CV is 20-40% on average (Fig 3a) reaching values around the 70% in specific months of the year (Fig. 3b). Such high values area reached in spring in northern Europe, in winter in the Mediterranean region, in summer in the Sahel region and in Southern Africa. Again, the CEFI variability is much larger than the mean daily estimation error. Its robustness further increases with the number of monthly estimations used to compute the median.

https://doi.org/10.5194/essd-2026-296
Preprint. Discussion started: 7 July 2026

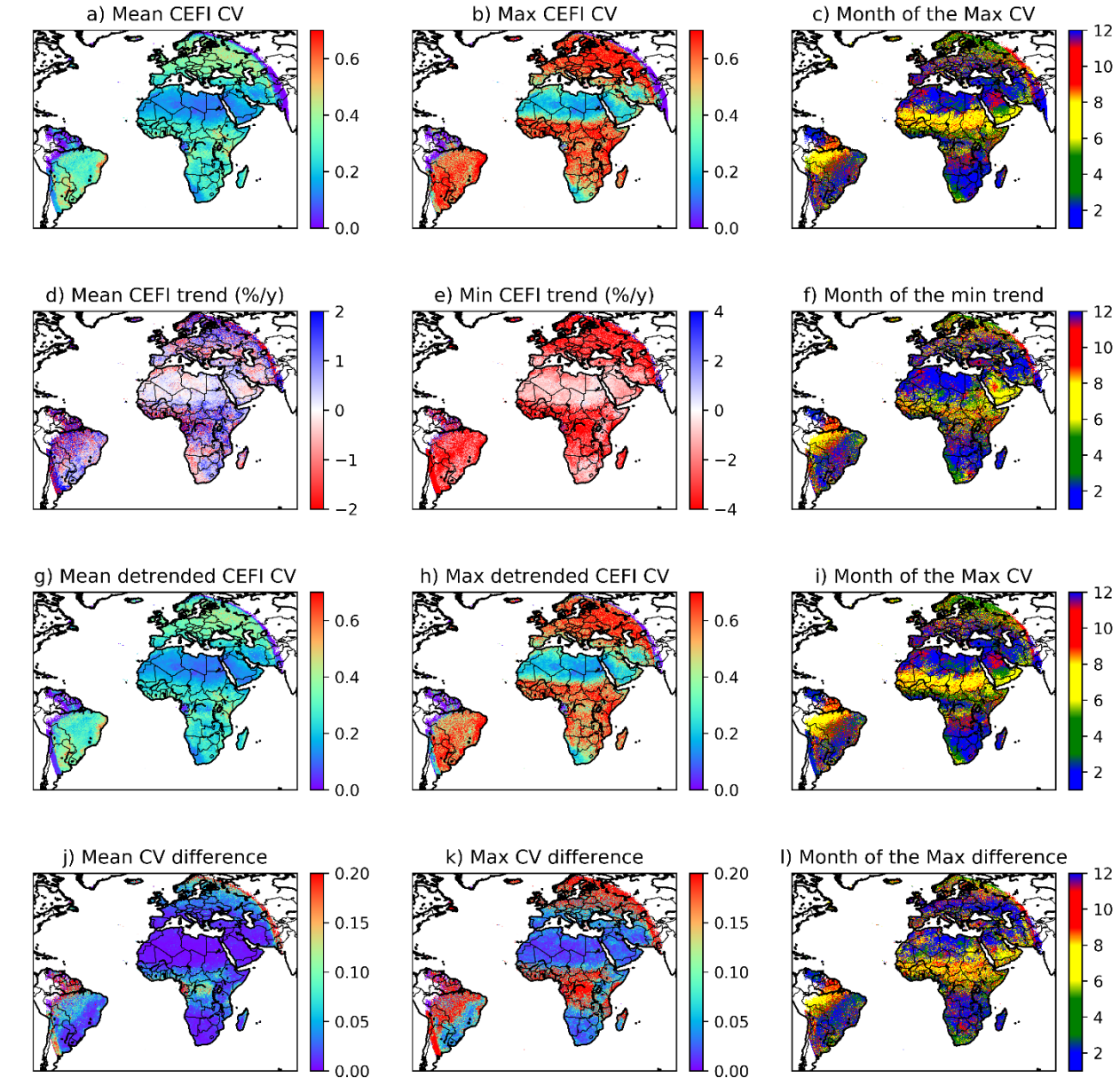

200

Figure 3: mean, max and month of the maximum CEFI Coefficient of Variation (CV, panels abc), trend (panels def), CV of the detrended CEFI timeseries (panels ghi) and difference between the CV of the original and detrended CEFI timeseries (jkl).

The CEFI does not display a clear trend in general (Fig 3d), but there are specific months of the year in which it is
205 consistently decreasing (Fig 3e). Interestingly, the period of the year with maximum decreasing trend (Fig 3f) almost coincides with the period with maximum CV (Fig 3c). This motivates repeating the analysis of the CV after removing the

https://doi.org/10.5194/essd-2026-296
Preprint. Discussion started: 7 July 2026

trend (Fig 3ghi). This analysis highlights the areas where the trend is significantly affecting the variability, which are the tropics and the high-latitudes (Fig 3jk). A significant reduction in CEFI variability in the tropics is consistently linked to the decreasing CEFI trend in summer (Fig 3l), highlighting a possible increase in aridity of those regions.

4.2 Spatial and temporal patterns of the CEFI

4.2.1 CEFI and meteorological drought

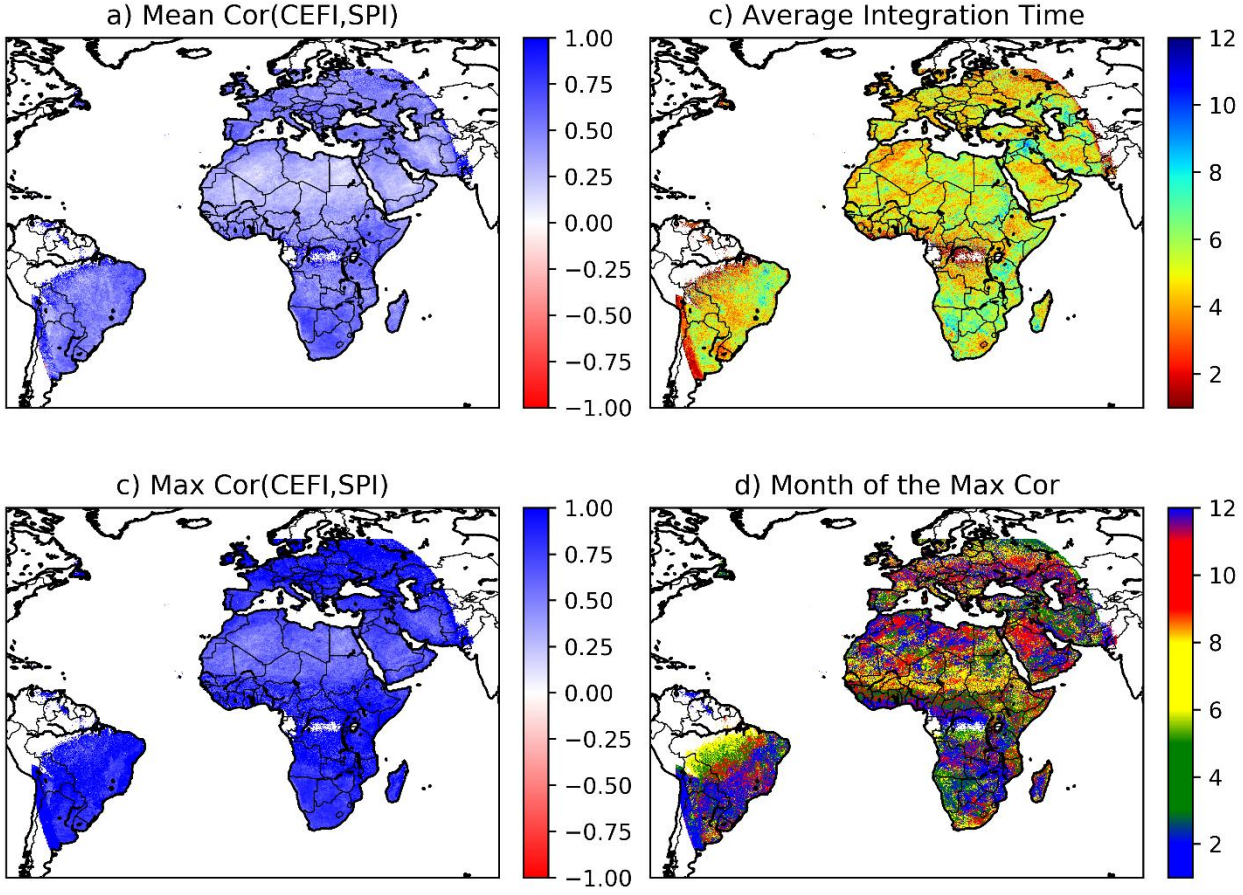

Figure 4: mean and max correlation and month of the maximum correlation between the CEFI a) correlation between the CEFI and the Standardized Precipitation Index (SPI) in all months, b) average SPI timescale corresponding to the correlation displayed in panel a, c) maximum correlation between the CEFI and the SPI, and d) the month of the maximum correlation depicted in panel c.

https://doi.org/10.5194/essd-2026-296
Preprint. Discussion started: 7 July 2026

The Standardized Precipitation Index (SPI) is a widely used multiscalar meteorological drought indicator that measures precipitation anomalies over varying time scales, typically ranging from 1 to 48 months. It is designed to be flexible, allowing users to analyze different types of droughts—short-term (e.g., 1–3 months) for agricultural moisture, and long-term (e.g., 12–48 months) for hydrological resources like groundwater and reservoirs.

The CEFI is positively correlated with the SPI almost everywhere, with the only exception of hyper arid regions (Figure 4a). This figure is computed using the SPI timescale that maximized the correlation with the CEFI for each month, and then averaging over all months of the year. This timescale is varying for each location from about 4 to 6 months (Figure 4b), reflecting the different interactions between the local hydrological processes and the surface turbulent fluxes. There are regions where the SPI timescale maximizing the correlation with the SPI is consistently larger, such as in Mesopotamia, probably because of the intense water management. The correlation in non-arid areas, already significantly high, is almost perfect for at least one month of the year (Figure 4cd), indicating a strong coupling between the integrated precipitation anomalies and the surface cooling efficiency and reinforcing the idea that the CEFI can be considered a proxy for drought stress during critical periods of the year.

4.2.2 CEFI and biophysical variables

The CEFI tends to be on average positively correlated with the surface soil moisture retrieved from the ESA CCI (Fig. 5a), the correlation greatly increases on specific months (Fig 5ab), when the soil moisture is a limiting factor for evapotranspiration. As already demonstrated by Zampieri et al. (2025), over non arid areas and far from the tropics, the CEFI is on average well correlated with monthly NDVI (Fig. 5d) and the GLEAM stress factor (Fig. 5g), which is defined similarly to the evaporative fraction, i.e. the ratio between actual and potential evapotranspiration (ET/ET_0, Miralles et al., 2025). While the average correlations between the CEFI and the GLEAM stress factor can be negative in overly dry and wet areas (as well as close to the MSG disk border, Fig. 5dg), there is almost always a month with positive and often very high correlation (Fig. 5eh). The month of the year in which the highest correlation is found is very similar between the ESA-CCI soil moisture (Fig. 5c), the MODIS NDVI (Fig. 5f) and the GLEAM stress factor (Fig. 5i). This reflects the high level of coupling between the vegetation stress and greenness reduction estimated by the GLEAM and NDVI datasets and the surface cooling efficiency anomalies estimated by the CEFI during specific periods of the year. This strong coupling between ecohydrological variables occurs in spring in the Mediterranean and South Africa, late summer in the Sahel region and in most of central Europe, for instance.

In addition to Zampieri et al. (2025), we demonstrate here the strong coupling between the CEFI and surface wind (Fig. 5j), which is on average stronger in arid regions, where the regulatory effect of vegetation of evapotranspiration is missing, but also in some parts of Europe. As it occurs for the vegetation related variables, it is always possible to find one month of the year is which the correlation is very high almost everywhere (Fig. 5k). This finding suggests that in some conditions the CEFI could be used as proxy of wind, especially over arid regions, which would be another innovative and unique

https://doi.org/10.5194/essd-2026-296
Preprint. Discussion started: 7 July 2026

application of satellite data over land. The month of the maximum coupling between the CEFI and wind is generally different than that for drought and the other vegetation related variables (Fig. 5l), being found sometimes in winter rather than in the summer months.

255

https://doi.org/10.5194/essd-2026-296
Preprint. Discussion started: 7 July 2026

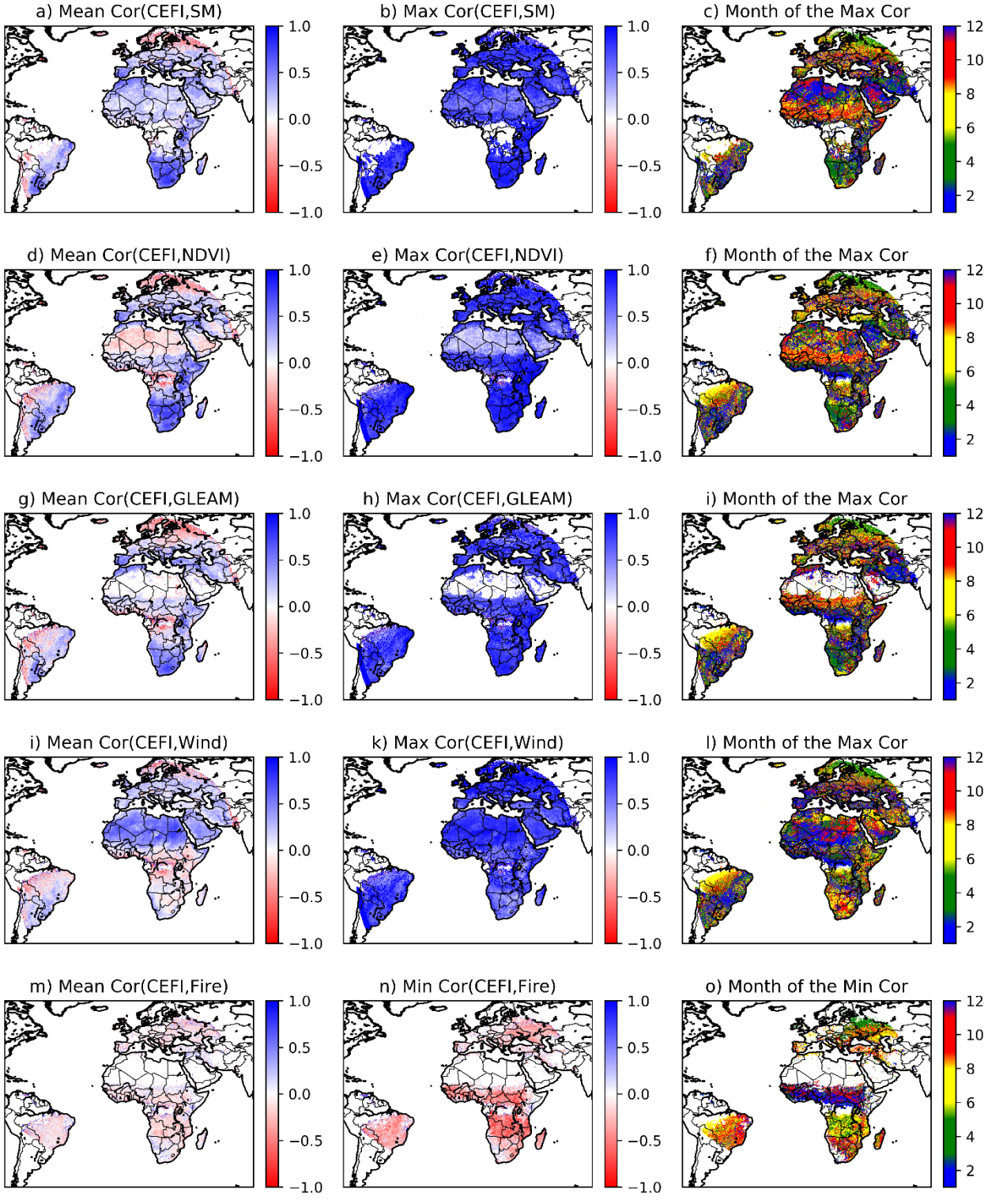

https://doi.org/10.5194/essd-2026-296
Preprint. Discussion started: 7 July 2026

Figure 5: mean and max correlation and month of the maximum correlation between the CEFI and abc) ESA-CCI soil moisture, def) MODIS NDVI, ghi) the GLEAM Stress factor and jkl) the ERA5-Land mean surface wind at the same time as the CEFI acquisitions. mno) mean and min correlation and month of the minimum correlation between the CEFI and the burned area fraction from MODIS.

We also tested the potential ability of the CEFI to estimate fire risk (Fig. 5mno). In this case, the correlation between the CEFI variability and the burned area frequencies is generally weaker (Fig. 5m), given the seasonal and sporadic nature of fire events that could also be of anthropogenic origin. However, is again possible to identify specific months of the year in which the correlation is stronger, negative in this case (Fig. 5n). The CEFI is highly correlated to the burned area in the Mediterranean and the Black Sea regions in summer and late summer, in the Sahel in Autumn, in Southern Africa and South America during the Austral spring (Fig. 5o).

4.2.3 CEFI and crop production

The use of the CEFI as drought indicator is supported by its strong correlation with traditional drought indicator such as the SPI (Fig. 4), and further strengthened by its links to observed surface soil moisture (Fig 5abc) as well as vegetation related variables (Fig 5defghi). A main role of drought indicators consists in monitoring and predicting crop production risk (e.g. Zampieri et al. 2017). In this case, the possible role of the CEFI consists in the direct estimation of vegetation stress, whether it is drive by soil moisture deficit or by enhanced atmospheric moisture demand as it happens in the case of heat waves (Zampieri et al. 2017). A precise estimation link between climate indicators and crop production anomalies is hindered by the fact that crop production data is often provided at the national level, while the climate anomalies need to be considered at the field level, considering the spatial distribution as well as the precise phenological stages when the crop is most sensitive, which are depending on the specific crop (Zampieri et al. 2017, 2019a). In some cases, different hydrological indicators rather that precipitation deficit needs to be accounted for (Zampieri et al., 2018, 2019b). Over Africa, maize is one of the most important staple food, South Africa being the larger producer and also an international player in the global food commodity market. Maize in Africa is very sensitive to drought, especially in the last part of the growing season excluding the harvesting month when the crop is left in the field to dry up. Drought during the harvesting month of maize is actually beneficial (Zampieri et al. 2019a).

https://doi.org/10.5194/essd-2026-296
Preprint. Discussion started: 7 July 2026

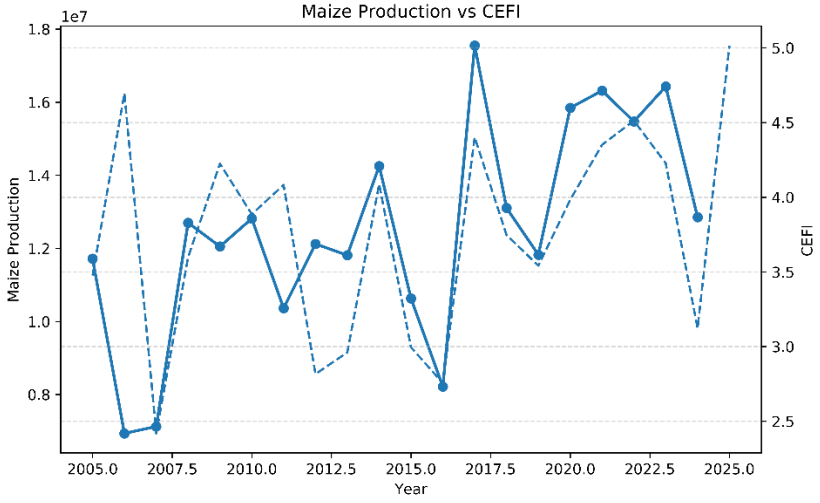

Figure 6: maize production in South Africa according to the FAOSTAT dataset (solid lines) and mean CEFI averages over the maize production area (25E - 30E, 22S - 30S) from February to April (dashed line).

The average CEFI is computed over the maize production area in South Africa on the last two months of the maize growing season leaving out the harvesting month and compared to the production record reported by FAOSTAT (Fig. 6). Maize production time-serie in South Africa indicates steadily increased since 2005, but it also large interannual variability. The CEFI reports, with few exceptions, the same variability and partly the same positive trend. After removing the suspicious outlier in 2006, the correlation between the CEFI and maize production in South Africa reaches 0.79, a level that is hardly found in studies linking climate indicators to crop production, despite the very rough estimation of the spatial averages implemented here (see e.g. Zampieri et al. 2017, 2018, 2019ab). The production values for 2025 are not available yet from the FAOSTAT dataset. However, the CEFI predicts a very positive yield.

4.2.4 CEFI and dust production

The use of the CEFI as proxy of surface wind anomalies is strongly supported by the correlation analysis between the CEFI and the average 10 meter wind computed during the CEFI estimation time window (Fig. 5jkl). Here we analyze the spatial correlation between the CEFI in the North Africa and Middle East and the dust aerosol optical depth in May, a period of the year with large dust concentration in the atmosphere, provided by the CAMS global reanalysis (EAC4).

https://doi.org/10.5194/essd-2026-296
Preprint. Discussion started: 7 July 2026

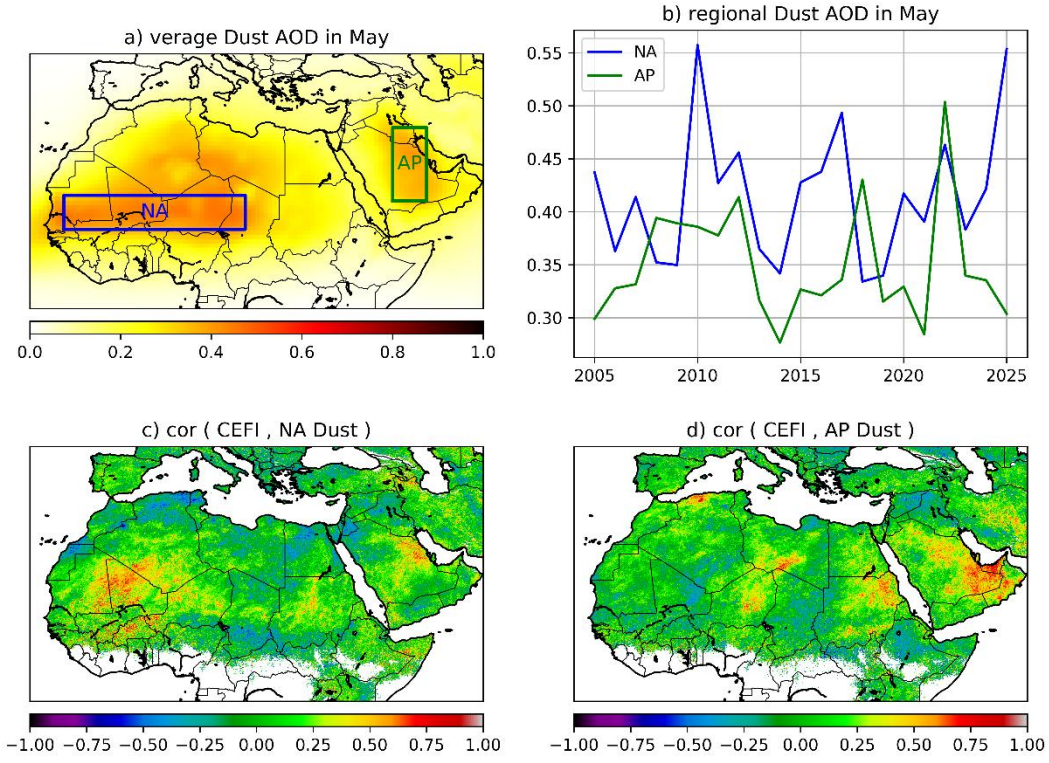

Figure 7: a) Dust Aerosols Optical Depth (DAOD) at 550nm in May (2005-2025 average), b) spatial DAOD averages over Norther Africa (NA, in blue) and the Arabia Peninsula (AP, green). Spatial correlation between the CEFI and c) the NA DAOD and d) the AP DAOD time series.

In May, the Intertropical Convergence Zone (ITCZ) reaches the Sahel region. Here the ITCZ represents the convergence between the South African monsoon and the Harmattan and Shamal northerly winds, which constitute the surface return flow of the Hadley circulation over the MENA region. These winds, blowing over the desert regions accumulate dust southwest to the dust formation zone, along the western Sahel region (Fig. 7a). On the other hand, dust production over the Empty Quarter can be brought to the center of the Peninsula by transient weather systems counteracting the mean Shamal wind. The correlation analysis between the DAOD time series (Fig. 7b) and the CEFI identify spatially coherent areas in North Africa (Fig. 6c) and the Middle East (Fig. 7d), which are usually associated to dust production. Some of these spatial patterns, such as the positive correlation between AP DAOD and the CEFI over North Africa could be due to non-causal correlation associated to the synoptic circulation regimes over the region. However, the overall pattern identified by this quick

https://doi.org/10.5194/essd-2026-296
Preprint. Discussion started: 7 July 2026

showcasing analysis is realistic. More precise analysis probably needs to consider daily data, in order to provide a useful dust risk product. However, as such, the CEFI can be used as a unique proxy of surface wind for dust production in desert regions – a metric otherwise non available from a purely observational point of view. Therefore, the CEFI could be used as a novel framework to better constrain and improve weather, climate and air quality models in arid regions.

320

4.2.5 Cities cooling Efficiency

The CEFI can be computed over every land cover types including urban regions. It is therefore possible and interesting to evaluate it over the main cities covered by the MSG disk (Fig. 8a). Only cities with an area of at least 100 square kilometers, roughly corresponding to four CEFI grid cells, were considered. This selection, applied to ensure a robust CEFI estimation,
325 reduces the sample to 245 cities. The median CEFI over such cities is 4.2 Wh m^{-2} K^{-2}, with interquartile range between 3.4 and 5.6 Wh m^{-2} K^{-2}. This range, as is can be expected, is more narrow than that displayed by the entire dataset considering all land cover types. However, very large values can be found over the coasts, most probably because of sea water surfaces partially included in the MSG grid used to compute the CEFI. Preliminary work identifies the annual precipitation, surface waters fraction and vegetation fraction as the better explanatory variables for the CEFI variability between different cities.
330 For previously unexplained reasons, research has found that heat waves in London are riskier for human health than other European cities such as Copenhagen (Chen et al. 2024). We find that London has CEFI = 3.3 Wh m^{-2} K^{-2} while Copenhagen has CEFI = 4.8 Wh m^{-2} K^{-2}. This remarkable difference of cooling efficiency between the two cities can explain the different sensitivity of human health between similar heat waves in these and other cities. Using the CEFI can help understand how city planning can be used as climate adaptation mechanism in the context of climate change.

335

https://doi.org/10.5194/essd-2026-296
Preprint. Discussion started: 7 July 2026

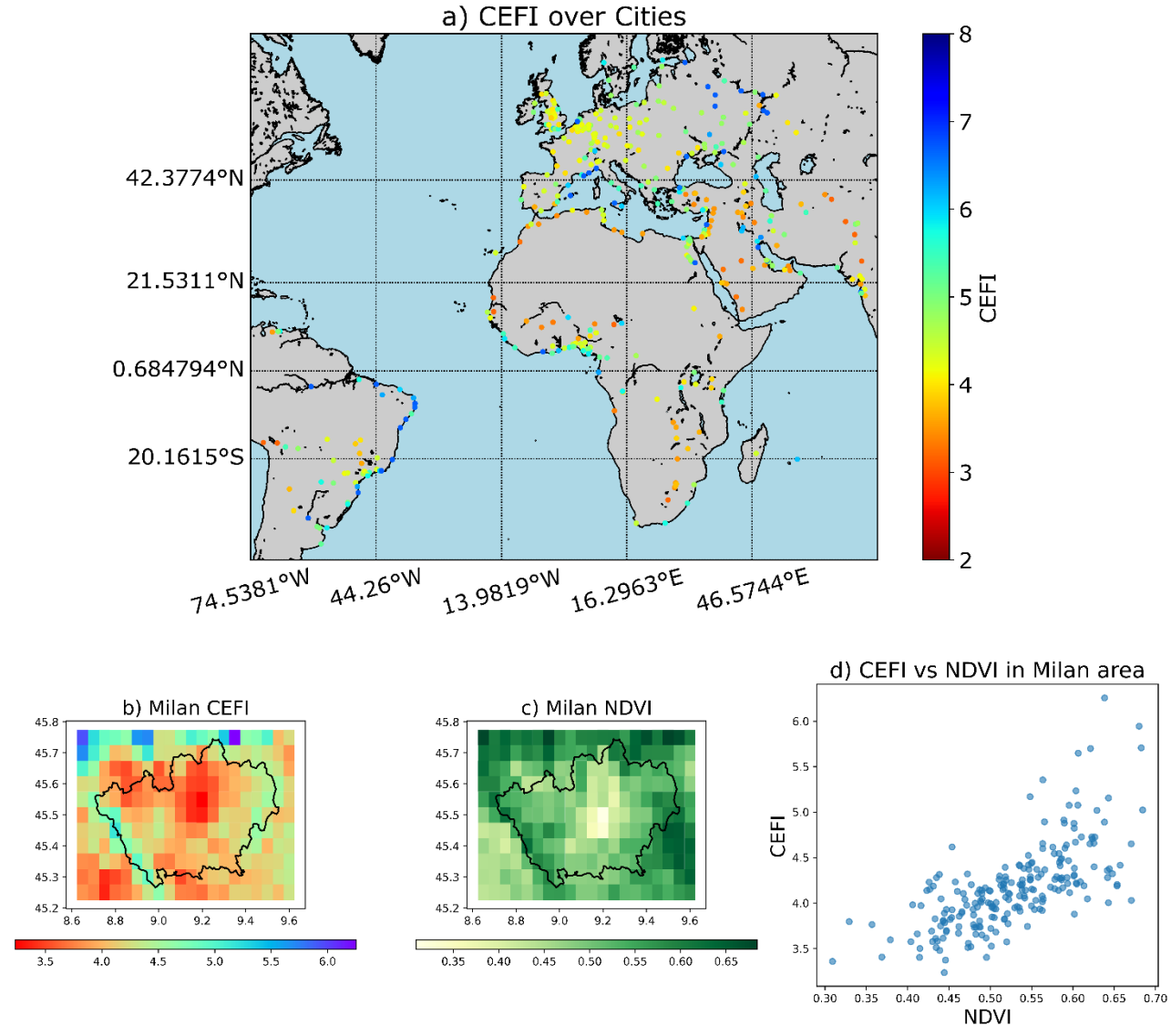

Figure 8: a) mean CEFI over cities with at least 100 square km area (minimum 4 CEFI grids per city). Spatial distribution of b) the CEFI and c) NDVI over the greater Milan area and d) their scatter plots.

The CEFI can be also used to understand within-city variability of the cooling efficiency, for sufficiency larger cities. For Milan (Fig 8bcd), for instance, the CEFI methodology confirms the contrast between vegetation and urban land cover fraction that produces the well-known "urban heat island" effect. In the greater Milan area, our analysis confirms that the CEFI is extremely well correlated with the vegetation distribution, represented here by the NDVI.

https://doi.org/10.5194/essd-2026-296
Preprint. Discussion started: 7 July 2026

5 Discussion

Drought is a persistent and increasing source of tension, conflict, and migration, particularly in developing countries (Eklund et al. 2022). Each year, drought causes global economic losses of about $500 billion (Sadoff et al. 2015), largely due to crop failure, livestock loss, reduced forest growth, soil and ecosystem degradation, wildfires, deteriorating air and water quality, and reduced hydropower generation and other industrial outputs (e.g. Zampieri et al. 2017, Turco et al. 2017, Liu et al. 2023). In addition, dry soils significantly increase the risk of heatwaves, which pose further risks to human health and further intensify drought conditions through a feedback loop (Seneviratne et al. 2010, Zampieri et al. 2024).

In response to the urgent need for a globally coordinated early warning system, numerous drought monitoring and forecasting initiatives have been developed worldwide (e.g. Rembold et al. 2023, Biella et al. 2026), with new systems emerging that focus on less-studied regions (e.g. Hoteit et al. 2025). These systems aim to monitor multiple dimensions of drought, including meteorological, soil moisture, agricultural/vegetation, and hydrological drought. They rely on combined and integrated indicators to account for the systemic nature of drought (Hagenlocher et al. 2023) and to maximize predictive capability (Shyrokaya et al. 2025).

However, drought monitoring is often based on estimated hazard anomalies rather than direct impact indicators, as drought is inherently a multiscale process characterized by a sequence of events that is not yet fully understood and still requires fundamental research (AghaKouchak et al. 2023). Meteorological drought is traditionally defined by negative precipitation anomalies, which act as the initial trigger. These anomalies are commonly quantified using the Standardized Precipitation Index (SPI), which enables comparison across different climatic regions (McLee et al., 1993). The SPI has been extended to include potential evapotranspiration, resulting in the Standardized Precipitation Evapotranspiration Index (SPEI, Vicente-Serrano et al. 2010). The SPEI serves as a proxy for surface water balance anomalies and is sensitive to climate change (Vicente-Serrano et al. 2010). However, both SPI and SPEI require calibration of thresholds and selection of appropriate accumulation periods to assess the risk of specific impacts.

With regard to vegetation impacts, soil moisture is often considered the most relevant indicator of drought stress (Liu et al. 2020). However, both direct and indirect observations of soil moisture remain challenging. Direct measurements using the gravimetric method are extremely rare and spatially inconsistent (Dorigo et al., 2021). Indirect estimates from microwave remote sensing represent only a very shallow surface layer (Kerr et al., 2016). Variability in deeper soil moisture and groundwater can be inferred from the Gravity Recovery and Climate Experiment (GRACE), but its spatial resolution and accuracy are insufficient for detailed vegetation drought assessments (Reager et al. 2009). Moreover, the actual amount of soil moisture accessible to plants remains uncertain, due to poorly constrained rooting depths and limited knowledge of soil properties affecting water retention and accessibility (Gao et al., 2014, Fan et al. 2017, Tariq et al. 2024).

The complexity increases further because vegetation drought stress is not solely determined by soil moisture but also by atmospheric vapor pressure deficit (VPD), a variable that is rarely available from direct observations (Novick et al. 2016, Grossiord et al. 2020, Novick et al. 2024). This is particularly relevant for flash droughts, an emerging climate change-

https://doi.org/10.5194/essd-2026-296
Preprint. Discussion started: 7 July 2026

related phenomenon characterized by rapid onset (Pendergrasse et al. 2020). Critically, flash droughts are often driven by VPD conditions that are not captured by standard indicators such as SPI and SPEI, which are better suited to slowly evolving droughts (Otkin et al. 2018, Yuan et al. 2018, Lesinger and Tian 2022).

In this context, the CEFI dataset can help fill these gaps by providing a direct, observation-based method to detect whether vegetation is under drought stress conditions. The CEFI is well correlated with, yet substantially distinct from, the aforementioned drought indicators. Therefore, the CEFI not only enhances the effectiveness of drought monitoring systems, but also opens new avenues for scientific research and potential applications. These include the estimation of fire risk in vegetated regions, crop production in agricultural areas, surface wind and dust production in arid environments, and the assessment of urban structure effectiveness for climate mitigation.

To our knowledge, no spatially distributed wind observations exists. Therefore, wind applications rely on poorly constrained modelling products. In this respect the CEFI can be used to better constrain the surface parameters and the turbulence parameterization of atmospheric models, advancing significantly meteorological forecast and climate projections as well as applications wind power generation and air quality estimations.

Fire risk monitoring is currently based on combined indicators such as the Fire Weather Index (FWI) developed by the Canadian Forest Service in the late 1960s, as well as similar methodologies that inform of the favourable meteorological conditions to triggering a wildfire (He et al. 2025). In this respect, this paper demonstrated that the CEFI can provide additional information purely based on observations of the actual status of vegetation drought stress, possibly incrementing the accuracy of the fire risk monitoring systems.

Moreover we have shown a very promising example of application of the CEFI in agriculture, which is a very important component of the global society that is under threat because of climate change. Generally, it was understood that climate variability could affect about one third of the main crops' production (Ray et al. 2015). Subsequent research has demonstrated that accurate indicators could explain a larger share of the interannual variability, 42% for wheat and 50% for maize (Zampieri et al. 2017, 2019a). The simple and rough estimation reported in this paper achieved 64% for maize in South Africa. Therefore, including the CEFI in more sophisticated methodologies accounting for detailed spatial distribution of the crops' phenological phases such as the Combines Stress Index (CSI, Zampieri et al. 2017, 2019a) can probably improve the performances of crop production anomalies estimation, with important implications for global food security.

Last but not least, we demonstrated the potential application of the CEFI for the urban areas. This is particularly important because, about 55–57% of the world's population already lives in urban areas, a share projected to rise to nearly 70% by 2050 (Massaro et al. 2023). Cities concentrate people, infrastructure, and economic activity, making them highly exposed to climate risks such as heatwaves, flooding, water scarcity, and air pollution, which can amplify social inequalities. This makes urban climate adaptation such resilient infrastructure, green spaces, improved water management, and heat mitigation, essential to protect lives, sustain economic productivity, and ensure livable cities under a changing climate. In this context, the CEFI can provide an observational constraint to evaluate the cities' cooling efficiency quantifying the relative roles of the fundamental properties that enhance the climate adaptation potential.

https://doi.org/10.5194/essd-2026-296
Preprint. Discussion started: 7 July 2026

6 Conclusions

The Cooling Efficiency Factor Index (CEFI) is an observational dataset that quantifies the land surface energy dissipation through turbulent and ecohydrological processes. It is defined based on diurnal variations in apparent heat capacity, a land surface property derived from geostationary satellite data acquired by the EUMETSAT's Meteosat Second Generation (MSG) program. The dataset is available from 2005 onward and covers Europe, Africa, and parts of West Asia and South America at a spatial resolution of 5 km. The spatial variability of the CEFI reflects differences in land surface properties, including surface roughness, vegetation cover, and water availability. Its temporal variability primarily serves as a proxy for drought stress events over vegetated regions and for wind speed anomalies over bare ground. Similarly to other satellite data, the use of CEFI also comes with some caveats, particularly related to the limited number of valid daily estimates requiring clear-sky conditions, which decreases substantially in tropical regions and at high latitudes. The operational application of CEFI should therefore be conducted with awareness of the variability in the number of daily estimates used to derive monthly CEFI values. An advantage of the CEFI compared to other satellite data is the robust estimation of the acquisitions error. The large coefficient of variation compared with the relative error suggests that the observed variability is not dominated by estimation uncertainty. In this respect, we have preliminarily demonstrated how the CEFI can be applied to assess natural vegetation and agricultural drought stress and productivity anomalies, wind-driven turbulence, fires, dust emission, and urban thermal behavior. Its strong consistency with established datasets such as CHIRPS, ESA-CCI soil moisture, MODIS NDVI, GLEAM stress factor, ERA5-Land 10 m wind speed, MODIS burned area, FAOSTAT crop production anomalies, and dust activity from the CAMS global reanalysis (EAC4) demonstrates that CEFI is a physically grounded integrative variable capable of revealing otherwise difficult-to-observe processes, especially in near real time. Because the index is fully observation-based, continuously updated, and globally scalable wherever suitable geostationary satellite data are available, CEFI has the potential to become a practical tool for climate monitoring, early warning systems, model evaluation and development, and adaptation planning in a warming world.

Data availability

The CEFI dataset can be downloaded from the JRC Data Catalogue (Zampieri and Cescatti, 2026, DOI: https://doi.org/10.2905/JRC.401M4D8). All supporting datasets used in this study to derive the CEFI or to validate it are publicly available and accessible through open repositories, ensuring full transparency and reproducibility.

Author contributions

AC conceived the idea. MZ formalized it and carried out the main analysis. MG, SMS, GC provided data, EM, MM and IH helped with the analysis. MZ prepared the manuscript with contributions from all co-authors.

https://doi.org/10.5194/essd-2026-296
Preprint. Discussion started: 7 July 2026

Competing interests

The authors declare no competing interests.

Disclaimer

Copernicus Publications remains neutral with regard to jurisdictional claims made in the text, published maps, institutional affiliations, or any other geographical representation in this paper. While Copernicus Publications makes every effort to include appropriate place names, the final responsibility lies with the authors. Views expressed in the text are those of the authors and do not necessarily reflect the views of the publisher.

Financial support

This work is funded by the Intra-ACP Climate Service and Related Application programme – ClimSA (Grant number: ACP/FED/038-833). M.Z. is also supported by the Climate Change Center, a partnership between the National Center of Meteorology (NCM) of Saudi Arabia and the King Abdullah University of Science and Technology (KAUST).

Review statement

The review statement will be added by Copernicus Publications listing the handling editor as well as all contributing referees according to their status anonymous or identified.

Acknowledgements

The authors acknowledge the use of AI-based language tools to improve the clarity and readability of the manuscript. All content has been carefully reviewed, and the authors take full responsibility for the final version.

References

AghaKouchak, A., Huning, L.S., Sadegh, M. et al.: Toward impact-based monitoring of drought and its cascading hazards. Nat Rev Earth Environ 4, 582–595. https://doi.org/10.1038/s43017-023-00457-2, 2023.

Alkama, R. and A. Cescatti: Biophysical climate impacts of recent changes in global forest cover, Science 351,600-604,.DOI:10.1126/science.aac8083, 2016

Arya, S. P. (2001). Introduction to Micrometeorology. Academic Press.

https://doi.org/10.5194/essd-2026-296
Preprint. Discussion started: 7 July 2026

Biella, R., Shyrokaya, A., Pechlivanidis, I., Cid, D., Llasat, M. C., Tootoonchi, F., Wens, M., Lam, M., Stenfors, E., Sutanto, S., Ridolfi, E., Ceola, S., Alencar, P., Di Baldassarre, G., Ionita, M., de Brito, M. M., McGrane, S. J., Moccia, B., Nagavciuc, V., Russo, F., Krakovska, S., Todorovic, A., Trambauer, P., Vignola, R., and Teutschbein, C.: Lessons learned in institutional preparedness and response during the 2022 European drought, Nat. Hazards Earth Syst. Sci., 26, 955–979, https://doi.org/10.5194/nhess-26-955-2026, 2026.

Brás T.A., Seixas J., Carvalhais N., J. Jägermeyr: Severity of drought and heatwave crop losses tripled over the last five decades in Europe, Environ. Res. Lett., 16, Article 065012, 10.1088/1748-9326/abf004, 2021

Chen, K., de Schrijver, E., Sivaraj, S. et al.: Impact of population aging on future temperature-related mortality at different global warming levels. Nat Commun 15, 1796, https://doi.org/10.1038/s41467-024-45901-z, 2024

Ciais, P., Reichstein, M., Viovy, N. et al.: Europe-wide reduction in primary productivity caused by the heat and drought in 2003. Nature 437, 529–533, https://doi.org/10.1038/nature03972, 2005

Duveiller, G., Hooker, J. and A. Cescatti: The mark of vegetation change on Earth's surface energy balance Nat Commun 9, 679, https://doi.org/10.1038/s41467-017-02810-8, 2018

Eklund, L., Theisen, O.M., Baumann, M. et al.: Societal drought vulnerability and the Syrian climate-conflict nexus are better explained by agriculture than meteorology. Commun Earth Environ 3, 85, https://doi.org/10.1038/s43247-022-00405-w, 2022

Fan Y., G. Miguez-Macho, E.G. Jobbágy, R.B. Jackson, C. Otero-Casal, Hydrologic regulation of plant rooting depth, Proc. Natl. Acad. Sci. 114 (40) 10572-10577, https://doi.org/10.1073/pnas.1712381114, 2017

Friedlingstein, P., O'Sullivan, M., Jones, M. W., Andrew, R. M., Gregor, L., et al. : Global Carbon Budget 2022, Earth Syst. Sci. Data, 14, 4811–4900, https://doi.org/10.5194/essd-14-4811-2022, 2022.

Gao, H., Hrachowitz, M., Schymanski, S., Fenicia, F., Sriwongsitanon, N., and Savenije, H.: Climate controls how ecosystems size the root zone storage capacity at catchment scale, Geophys. Res. Lett., 41, 7916–7923, 2014

Grossiord, C., Buckley, T.N., Cernusak, L.A., Novick, K.A., Poulter, B., Siegwolf, R.T.W., Sperry, J.S. and McDowell, N.G.: Plant responses to rising vapor pressure deficit. New Phytol, 226: 1550-1566. https://doi.org/10.1111/nph.16485, 2020

Hartmann, H., Bastos, A., Das, A.J., Esquivel-Muelbert, A., Hammond, W.M., Martínez-Vilalta, J., McDowell, N.G., Powers, J.S., Pugh, T.A.M., Ruthrof, K.X., Allen, C.D.: Climate Change Risks to Global Forest Health: Emergence of Unexpected Events of Elevated Tree Mortality Worldwide. Annu Rev Plant Biol.,73:673-702. doi: 10.1146/annurev-arplant-102820-012804, 2022

Hansen, M.C., Potapov, P.V., Moore, R., Hancher, M., Turubanova, S.A., Tyukavina, A., Thau, D., Stehman, S.V., Goetz, S.J., Loveland, T.R., Kommareddy, A., Egorov, A., Chini, L., Justice, C.O. and J.R.G. Townshend: High-Resolution Global Maps of 21st-Century Forest Cover Change.Science342,850-853,DOI:10.1126/science.1244693, 2013

He, Y., Zhou, Z., Im, E. S. & Kwon, H. H.: Wildfire risk in a changing climate: evaluating fire weather indices and their global patterns with CMIP6 multi-model projections. Weather Clim. Extremes. 48, 100751 https://doi.org/10.1016/j.wace.2025.100751, 2025

https://doi.org/10.5194/essd-2026-296
Preprint. Discussion started: 7 July 2026

500 Hoteit, I., Abualnaja, Y., Afzal, S., Aman, C., Antony, C., Ashok, K., et al.: New climate change center of Saudi Arabia: Advancing understanding and prediction for the Arabian Peninsula climate. Earth's Future, 13, e2025EF006296, https://doi.org/10.1029/2025EF006296 , 2025

Jung, M., Koirala, S., Weber, U. et al.: The FLUXCOM ensemble of global land-atmosphere energy fluxes. Sci Data 6, 74. https://doi.org/10.1038/s41597-019-0076-8, 2019

505 Justice, C. O., Giglio, L., Korontzi, S., Owens, J., Morisette, J., Roy, D., Descloitres, J., Alleaume, S., Petitcolin, F., and Kaufman, Y. J.: The MODIS fire products. Remote Sensing of Environment, 83:244-262, 2002

Li, Z.-L., Wu, H., Duan, S.-B., Zhao, W., Ren, H., Liu, X., et al.: Satellite remote sensing of global land surface temperature: Definition, methods, products, and applications. Reviews of Geophysics, 61, e2022RG000777. https://doi.org/10.1029/2022RG000777, 2023

510 Kerr, Y., Al-Yaari, A., Rodriguez-Fernandez, N., Parrens, M., Molero, B., Leroux, D., Bircher, S., Mahmoodi, A., Mialon, A., Richaume, P., Delwart, S., Al Bitar, A., Pellarin, T., Bindlish, R., Jackson, T., Rüdiger, C., Waldteufel, P., Mecklenburg, S., and Wigneron, J.-P.: Overview of SMOS performance in terms of global soil moisture monitoring after six years in operation, Remote Sens. Environ., 180, 40–63, https://doi.org/10.1016/j.rse.2016.02.042, 2016.

Lesinger, K., & Tian, D.: Trends, variability, and drivers of flash droughts in the contiguous United States. Water Resources

515 Research, 58(9), e2022WR032186. https://doi.org/10.1029/2022wr032186, 2022

Liu, L., Gudmundsson, L., Hauser, M. et al.: Soil moisture dominates dryness stress on ecosystem production globally. Nat Commun 11, 4892. https://doi.org/10.1038/s41467-020-18631-1, 2020

Liu X., Yuan X., Ma F., Xia J.: The increasing risk of energy droughts for hydropower in the Yangtze River basin, Journal of Hydrology, Volume 621, 129589, ISSN 0022-1694, https://doi.org/10.1016/j.jhydrol.2023.129589, 2023

520 Otkin, J. A., Svoboda, M., Hunt, E. D., Ford, T. W., Anderson, M. C., Hain, C., & Basara, J. B.: Flash droughts: A review and assessment of the challenges imposed by rapid-onset droughts in the United States. Bulletin of the American Meteorological Society, 99(5), 911–919. https://doi.org/10.1175/bams-d-17-0149.1, 2018

Massaro, E., Schifanella, R., Piccardo, M. et al.: Spatially-optimized urban greening for reduction of population exposure to land surface temperature extremes. Nat Commun 14, 2903. https://doi.org/10.1038/s41467-023-38596-1, 2023

525 Miralles, D., Teuling, A., van Heerwaarden, C. et al.: Mega-heatwave temperatures due to combined soil desiccation and atmospheric heat accumulation. Nature Geosci 7, 345–349. https://doi.org/10.1038/ngeo2141, 2014

McKay, D.I.A., Staal, A., Abrams, J.F., Winkelmann, R., Sakschewski, B., Loriani, S., Fetzer, I., Cornell, S.E., Rockström, J., Lenton, T.M..: Exceeding 1.5°C global warming could trigger multiple climate tipping points. Science. Sep 9;377(6611):eabn7950. doi: 10.1126/science.abn7950. Epub 2022 Sep 9. PMID: 36074831, 2022

530 McKee, T.B., Nolan J.D., and J. Kleist: The relationship of drought frequency and duration to time scales. Proceedings of the 8th Conference on Applied Climatology. Vol. 17. No. 22. 1993.

Mehrabi, Z., Tong, K., Fortin, J., Stanimirova, R., Friedl, M., and Ramankutty, N.: Global agricultural lands in the year 2015, Earth Syst. Sci. Data, 17, 3473–3496, https://doi.org/10.5194/essd-17-3473-2025, 2025.

https://doi.org/10.5194/essd-2026-296
Preprint. Discussion started: 7 July 2026

Miralles, D.G., Bonte, O., Koppa, A., Baez-Villanueva, O.M., Tronquo, E., Zhong, F., Beck, H.E., Hulsman, P., Dorigo, W.A., Verhoest, N.E.C., Haghdoost, S.: GLEAM4: global land evaporation and soil moisture dataset at 0.1° resolution from 1980 to near present, Scientific Data, 12, 416, 2025

Naumann, G., Alfieri, L., Wyser, K., Mentaschi, L., Betts, R., Saiote Carrao, H., Spinoni, J., Vogt, J. and Feyen, L.: Global changes in drought conditions under different levels of warming, Geophysical Research Letters, ISSN 0094-8276, 45 (7), p. 3285-3296, JRC106673, 2018

Novick, K. A. et al.: The increasing importance of atmospheric demand for ecosystem water and carbon fluxes. Nat. Clim. Change 6, 1023–1027, 2016

Novick, K.A., Ficklin, D.L., Grossiord, C., Konings, A.G., Martínez-Vilalta, J., Sadok, W. et al.: The impacts of rising vapour pressure deficit in natural and managed ecosystems. Plant, Cell & Environment, 47, 3561–3589. https://doi.org/10.1111/pce.14846, 2024

Pendergrass, A.G., Meehl, G.A., Pulwarty, R. et al.: Flash droughts present a new challenge for subseasonal-to-seasonal prediction. Nat. Clim. Chang. 10, 191–199, https://doi.org/10.1038/s41558-020-0709-0, 2020.

Pesaresi, M., Carneiro Freire, S., Ehrlich, D., Florczyk, A., Kemper, T., Julea, A., Soille, P., Syrris, V., Zanchetta, L.: Global Human Settlement Layer. European Commission, JRC102420, 2016

Pickens, A.H., Hansen, M.C., Song, Z. et al. : Rapid monitoring of global land change. Nat Commun 16, 8948. https://doi.org/10.1038/s41467-025-64014-9, 2025

Ray, D.K., Gerber, J.S., MacDonald, G.K., West, P.C.: Climate variation explains a third of global crop yield variability. Nat Commun. 6:5989. doi: 10.1038/ncomms6989, 2015

Reager, J. and J. Famiglietti: Global terrestrial water storage capacity and flood potential using GRACE. Geophys. Res. Lett. 36, 2009

Rembold, F., Meroni, M., Otieno, V., Kipkogei, O., Mwangi, K., de Sousa Afonso, J.M., Ihadua, I.M.T.J., José, A.E.A., Zoungrana, L.E., Taieb, A.H., et al.: New Functionalities and Regional/National Use Cases of the Anomaly Hotspots of Agricultural Production (ASAP) Platform. Remote Sens., 15, 4284. https://doi.org/10.3390/rs15174284, 2023

Reichstein, M., Bahn, M., Ciais, P. et al.: Climate extremes and the carbon cycle. *Nature* **500**, 287–295. https://doi.org/10.1038/nature12350, 2013

Sadoff, C.W., Hall, J.W., Grey, D., Aerts, J.C.J.H., Ait-Kadi, M., Brown, C., Cox, A., Dadson, S., Garrick, D., Kelman, J., McCornick, P., Ringler, C., Rosegrant, M., Whittington, D. and Wiberg, D. : Securing Water, Sustaining Growth: Report of the GWP/OECD Task Force on Water Security and Sustainable Growth, University of Oxford, UK, 180pp, 2015

Shen, P., Zhao, S., & Ma, Y.: Perturbation of urbanization to Earth's surface energy balance. Journal of Geophysical Research: Atmospheres, 126, e2020JD033521. https://doi.org/10.1029/2020JD033521, 2021

Shyrokaya, A., Pappenberger, F., Messori, G., Pechlivanidis, I., Cloke, H. L. and Di Baldassarre, G.: How good is my drought index? Evaluating predictability and ability to estimate impacts across Europe. Environmental Research Letters, 20 (3). 034051. ISSN 1748-9326 doi: 10.1088/1748-9326/adb869, 2025.

https://doi.org/10.5194/essd-2026-296
Preprint. Discussion started: 7 July 2026

Tariq, A. , Graciano C., Sardans J., et al.: Plant Root Mechanisms and Their Effects on Carbon and Nutrient Accumulation in Desert Ecosystems Under Changes in Land Use and Climate. New Phytologist 242: 916–934, 2024.

Trigo, I. F., Peres, L. F., DaCamara, C. C. and S. C. Freitas: Thermal Land Surface Emissivity Retrieved From SEVIRI/Meteosat, IEEE Transactions on Geoscience and Remote Sensing, 46(2), 307-315, doi: 10.1109/TGRS.2007.905197, 2008.

Trigo, I. F., Dacamara, C. C., Viterbo, P., Roujean, J. L., Olesen, F., Barroso, C., … Arboleda, A.: The Satellite Application Facility for Land Surface Analysis. International Journal of Remote Sensing, 32(10), 2725–2744. https://doi.org/10.1080/01431161003743199, 2011.

Turco, M., von Hardenberg, J., AghaKouchak, A. et al.: On the key role of droughts in the dynamics of summer fires in Mediterranean Europe. Sci Rep 7, 81. https://doi.org/10.1038/s41598-017-00116-9, 2017

Vicente-Serrano, S. M., Beguería, S., & López-Moreno, J. I. (2010). A multiscalar drought index sensitive to global warming: the standardized precipitation evapotranspiration index. Journal of climate, 23(7), 1696-1718.

Zampieri, M., F. D'Andrea, R. Vautard, P. Ciais, N. de Noblet-Ducoudré, and P. Yiou: Hot European Summers and the Role of Soil Moisture in the Propagation of Mediterranean Drought. J. Climate, 22, 4747–4758, https://doi.org/10.1175/2009JCLI2568.1, 2009

Yuan, X., Wang, L., & Wood, E. F.: Anthropogenic intensification of southern African flash droughts as exemplified by the 2015/16 season. Bulletin of the American Meteorological Society, 99(1), S86–S90. https://doi.org/10.1175/bams-d-17-0077.1, 2018

Zampieri, M., Ceglar, A., Dentener, F. and A. Toreti: Wheat yield loss attributable to heat waves, drought and water excess at the global, national and subnational scales, Environmental Research Letters 12 (6), 064008, 2017

Zampieri, M., Carmona Garcia, G., Dentener, F., Gumma, M., Salamon, P. et al.: Surface freshwater limitation explains worst rice production anomaly in India in 2002, Remote Sensing 10 (2), 244, 2018

Zampieri, M., Ceglar, A., Dentener, F., Dosio, A., Naumann, G., Van Den Berg, M., et al.: When will current climate extremes affecting maize production become the norm? Earth's Future 7 (2), 113-122, 2019a

Zampieri, M., Ceglar, A., Manfron, G., Toreti, A., Duveiller, G., Romani, M., et al.: Adaptation and sustainability of water management for rice agriculture in temperate regions: The Italian case-study, Land Degradation & Development, 30(17), 2033-2047, 2019b

Zampieri, M., Piccardo, M., Girardello, M., Ceccherini, G., Hoteit, I. and A.: Cescatti, Remote monitoring of plant drought stress with the apparent heat capacity, Science of The Total Environment 1000, 20 October 2025, 180391, 2025

Zampieri, M.; Cescatti, A.: CEFI v1.0. European Commission, Joint Research Centre [Dataset] doi: 10.2905/JRC.401M4D8 PID: http://data.europa.eu/89h/1e56ccfc-f9fa-4476-a92f-fccaeee7c19f, 2026